Three-Dimensional, Upwind, Parabolized Navier-Stokes Code for Chemically Reacting Flows

Philip E. Buelow,* John C. Tannehill,† and John O. Ievalts‡
Engineering Analysis, Inc., Ames, Iowa 50011
and
Scott L. Lawrence§
NASA Ames Research Center, Moffett Field, California 94305

A new upwind, parabolized Navier-Stokes (PNS) code has been developed to compute the three-dimensional viscous flow of chemically reacting air around hypersonic vehicles. The code is a modification of the perfect gas, three-dimensional UPS code of Lawrence et al., which has been extended in the present study to permit the calculation of hypersonic, viscous flows in chemical nonequilibrium. The algorithm solves the PNS equations using a finite-volume, upwind total variation diminishing (TVD) method based on Roe's approximate Riemann solver that has been modified to account for "real gas" effects. The present code solves the fluid dynamic and species continuity equations in a loosely coupled manner. The fluid medium is assumed to be a chemically reacting mixture of thermally perfect (but calorically imperfect) gases in thermal equilibrium. The code has been used to compute the hypersonic laminar flow of chemically reacting air over a cone at 0- and 10-deg angles of attack, and the results are compared with results from other existing upwind and central-difference, real gas PNS codes. In addition, the code has been used to compute the Mach 25 flow over a generic hypersonic vehicle.

Introduction

WITH the advent of the National Aero-Space Plane and fuel-efficient aeroassisted orbital transfer vehicles (AOTVs) has come a renewed interest in hypersonic aerothermodynamics. The experimental determination of flight characteristics, heating, and chemical effects on these vehicles represents an enormous task. As a result, a concerted effort has been directed toward the numerical simulation of these hypersonic flight conditions. Numerous numerical methods have been proposed that solve either the unsteady Navier-Stokes (NS) equations[1-8] or the steady parabolized Navier-Stokes (PNS) equations.[8-22] The unsteady NS solvers are required to solve the flow around AOTVs and other blunt-nosed hypersonic vehicles, where the PNS equations are not well posed. Aft of the nose region, the PNS equations are a valid set provided the inviscid region of the flow is supersonic and there is no streamwise flow separation. Depending on the flight conditions, the fluid medium may be in thermochemical equilibrium, chemical nonequilibrium, or thermochemical nonequilibrium.

To account for nonequilibrium effects, chemical reactions must be modeled along with the fluid dynamics. Two different procedures can be used: 1) strong coupling between the fluids and the chemistry, or 2) weak coupling between the fluids and the chemistry, also referred to as loosely coupled. In the strongly coupled approach, the fluids and chemistry are solved simultaneously as a single-equation set. This provides an immediate influence of the chemistry on the fluids and vice versa. However, as the chemical model increases in complexity (i.e., the number of reactions and reactants increases), the solution of such large systems becomes computationally expensive as a result of having to invert large block matrices. In the loosely coupled approach, the fluids are solved separately from the chemistry, and the coupling between the two is performed in either an approximate or iterative manner. Here, as the complexity of the chemical model increases, only the chemistry solution is affected; the solution procedure for the fluids remains essentially unaltered. Another advantage is that the system of equations for the chemistry can be solved in an uncoupled fashion, thus eliminating the need for block inversions for the chemistry step.

Using the loosely coupled approach, Tannehill et al.[17] have extended the two-dimensional version of the Lawrence et al.[23] UPS code to permit nonequilibrium computations. More recently, the perfect gas version of the three-dimensional (3-D) UPS code[24] has been extended to permit equilibrium air calculations.[21] In the present study, the 3-D UPS code is further extended to permit nonequilibrium (finite-rate chemically reacting) air calculations. The fluid dynamic equations are solved in a loosely coupled manner with the species continuity equations, in much the same manner as Tannehill et al.[17] The coupling is provided for in an approximate manner that can be iterated, if necessary. The fluid medium is assumed to be a chemically reacting mixture of thermally perfect gases in thermal equilibrium. The loosely coupled approach was chosen because it is a convenient way to extend the perfect gas version of the 3-D UPS code to nonequilibrium (only minor modifications were necessary to the fluid dynamic equations). As a result of this approach, the code has been structured such that one can efficiently perform a perfect gas, equilibrium air, or chemical nonequilibrium air computation by changing just one input parameter.

Another advantage of the present approach lies in the fact that the convective terms in the governing equations are modeled in an upwind TVD manner that requires no user-specified

Presented as Paper 90-0394 at the AIAA 28th Aerospace Sciences Meeting, Reno, NV, Jan. 8-11, 1990; received Jan. 22, 1990; revision received Oct. 30, 1990; accepted for publication Oct. 30, 1990.

*Research Scientists; currently, Graduate Research Assistant, Department of Aerospace Engineering and Engineering Mechanics, Iowa State University, Ames, IA. Member AIAA.

†President; currently, Manager, Computational Fluid Dynamics Center and Professor, Department of Aerospace Engineering and Engineering Mechanics, Iowa State University, Ames, IA. Member AIAA.

‡Research Scientist; currently, Computing Consultant, Department of Aerospace Engineering and Engineering Mechanics, Iowa State University, Ames, IA. Member AIAA.

§Research Scientist, Applied Computational Fluid Dynamics Branch. Member AIAA.

dissipation terms. This enhances the robustness over standard centrally differenced codes that require user-specified dissipation, which can result in a polluted solution either due to severe flow property oscillations near discontinuities or excessive artificial dissipation needed to reduce these oscillations.

The resulting code has been used to compute the hypersonic, laminar flow of chemically reacting air over a 10-deg half-angle cone at 0- and 10-deg angles of attack. Comparisons are made with results from the strongly coupled, upwind PNS code (STUFF) of Molvik and Merkle,[8] and the strongly coupled, central-difference PNS code (TONIC) of Prabhu et al.[12] and Wadawadigi.[25] Results are also presented using the three gas models present in the code: perfect gas, equilibrium air, and chemical nonequilibrium air. In addition, the flow over the McDonnell Douglas Blended-Wing-Body (MDC-BWB) generic option hypersonic vehicle has been computed. For this case, comparisons are made among the three gas models at a flight condition corresponding to the high-speed, high-altitude end of the airbreathing flight corridor for a transatmospheric vehicle.

Governing Equations

The governing equations used to model the fluids are the PNS equations. The PNS equations are obtained from the compressible NS equations by dropping the unsteady terms and neglecting the streamwise viscous terms. The resulting nondimensional fluid dynamic set in generalized coordinates (ξ, η, ζ) is given by

$$\frac{\partial \boldsymbol{E}}{\partial \xi} + \frac{\partial \boldsymbol{F}}{\partial \eta} + \frac{\partial \boldsymbol{G}}{\partial \zeta} = 0 \tag{1}$$

where

$$\boldsymbol{E} = \left(\frac{\xi_x}{J}\right)\boldsymbol{E}_i + \left(\frac{\xi_y}{J}\right)\boldsymbol{F}_i + \left(\frac{\xi_z}{J}\right)\boldsymbol{G}_i \tag{2a}$$

$$\boldsymbol{F} = \left(\frac{\eta_x}{J}\right)(\boldsymbol{E}_i - \boldsymbol{E}_v^*) + \left(\frac{\eta_y}{J}\right)(\boldsymbol{F}_i - \boldsymbol{F}_v^*) + \left(\frac{\eta_z}{J}\right)(\boldsymbol{G}_i - \boldsymbol{G}_v^*) \tag{2b}$$

$$\boldsymbol{G} = \left(\frac{\zeta_x}{J}\right)(\boldsymbol{E}_i - \boldsymbol{E}_v^*) + \left(\frac{\zeta_y}{J}\right)(\boldsymbol{F}_i - \boldsymbol{F}_v^*) + \left(\frac{\zeta_z}{J}\right)(\boldsymbol{G}_i - \boldsymbol{G}_v^*) \tag{2c}$$

The inviscid and viscous vectors are defined by

$$\boldsymbol{E} = [\rho u, \rho u^2 + p, \rho uv, \rho uw, (E_t + p)u]^T \tag{3a}$$

$$\boldsymbol{F} = [\rho v, \rho uv, \rho v^2 + p, \rho vw, (E_t + p)v]^T \tag{3b}$$

$$\boldsymbol{G} = [\rho w, \rho uw, \rho vw, \rho w^2 + p, (E_t + p)w]^T \tag{3c}$$

$$\boldsymbol{E}_v = [0, \tau_{xx}, \tau_{xy}, \tau_{xz}, u\tau_{xx} + v\tau_{xy} + w\tau_{xz} - q_x]^T \tag{3d}$$

$$\boldsymbol{F}_v = [0, \tau_{xy}, \tau_{yy}, \tau_{yz}, u\tau_{xy} + v\tau_{yy} + w\tau_{yz} - q_y]^T \tag{3e}$$

$$\boldsymbol{G}_v = [0, \tau_{xz}, \tau_{yz}, \tau_{zz}, u\tau_{xz} + v\tau_{yz} + w\tau_{zz} - q_z]^T \tag{3f}$$

where

$$E_t = \rho\left[e + \frac{1}{2}(u^2 + v^2 + w^2)\right]$$

The superscript asterisk on the viscous vectors in Eqs. (2) indicates that derivatives with respect to ξ have been eliminated. In these equations, p is the pressure; ρ the density; u, v, and w the velocity components in the x, y, and z directions, respectively; e the internal energy; τ the viscous stress; μ the coefficient of viscosity; q the heat flux due to conduction; and κ the coefficient of thermal conductivity. The dependent variables are nondimensionalized as follows (dimensional quantities are denoted by a tilde):

$$u, v, w = \frac{\tilde{u}, \tilde{v}, \tilde{w}}{\tilde{V}_\infty}, \quad \rho = \frac{\tilde{\rho}}{\tilde{\rho}_\infty}, \quad T = \frac{\tilde{T}}{\tilde{T}_\infty}, \quad p = \frac{\tilde{p}}{\tilde{\rho}_\infty \tilde{V}_\infty^2}$$

$$e = \frac{\tilde{e}}{\tilde{V}_\infty^2}, \quad h = \frac{\tilde{h}}{\tilde{V}_\infty^2}, \quad \mu = \frac{\tilde{\mu}}{\tilde{\mu}_\infty}, \quad \kappa = \frac{\tilde{\kappa}}{\tilde{\kappa}_\infty} \tag{4}$$

The spatial coordinates (x, y, z) are left in their dimensional units.

The PNS equations are a mixed set of hyperbolic-parabolic equations in the streamwise direction ξ provided that the inviscid flow is supersonic, the streamwise velocity component is everywhere greater than zero, and the streamwise pressure gradient term is either omitted in subsonic regions or the "departure behavior" is suppressed by a suitable technique. In the present study, the technique of Vigneron et al.[26] is used to prevent departure solutions.

For chemical nonequilibrium airflows, the effects of mass diffusion must be included in the energy equation. This appears as a diffusion component added to the heat flux terms (q_x, q_y, q_z), so that the heat flux terms are now given by

$$\boldsymbol{q} = -\kappa \nabla T + \rho \sum_{s=1}^{n} c_s U_s h_s, \qquad s = 1, 2, \ldots, n \tag{5}$$

where U_s is the diffusion velocity of species s, c_s is the species mass fraction, h_s is the species enthalpy, and the subscript s indicates the species index $(s = 1, 2, \ldots, n)$.

The species continuity equations must also be solved. These equations are expressed as follows:

$$\frac{\partial \rho_s}{\partial t} + \nabla \cdot (\rho_s \boldsymbol{V}_s) = \dot{\omega}_s, \qquad s = 1, 2, \ldots, n \tag{6}$$

where

$$\boldsymbol{V}_s = \boldsymbol{V} + \boldsymbol{U}_s \tag{7}$$

The fluid velocity is denoted by $\boldsymbol{V}$, the species density is denoted by ρ_s, and $\dot{\omega}_s$ represents the rate of production of species. These equations are simplified through the use of the global continuity equation and the assumption of Fick's law for mass diffusion to yield the following form of the species continuity equations:

$$\rho\left[\frac{\partial c_s}{\partial t} + \boldsymbol{V} \cdot \nabla c_s\right] = \nabla \cdot (\beta_3 \rho D_{sm} \nabla c_s) + \dot{\omega}_s \tag{8}$$

where

$$\beta_3 = \frac{\tilde{\rho}_\infty \tilde{D}_\infty}{\tilde{\mu}_\infty Re_\infty} \tag{9}$$

and D_{sm} is the multicomponent diffusion coefficient for species s. The species continuity equations are further simplified (as in the case of the PNS equations) by dropping the unsteady term and neglecting the streamwise diffusion terms. The final nondimensional form of these equations written in generalized coordinates is

$$\rho\hat{U}\frac{\partial c_s}{\partial \xi} + \rho\hat{V}\frac{\partial c_s}{\partial \eta} + \rho\hat{W}\frac{\partial c_s}{\partial \zeta} - \frac{\partial}{\partial \eta}\left[A_{\eta\eta}\frac{\partial c_s}{\partial \eta} + A_{\eta\zeta}\frac{\partial c_s}{\partial \zeta}\right] - \frac{\partial}{\partial \zeta}\left[A_{\zeta\zeta}\frac{\partial c_s}{\partial \zeta} + A_{\zeta\eta}\frac{\partial c_s}{\partial \eta}\right] = \frac{\dot{\omega}_s}{J}, \qquad s = 1, 2, \ldots, n \tag{10}$$

where

$$\hat{U} = (\xi_x/J)u + (\xi_y/J)v + (\xi_z/J)w \tag{11a}$$

$$\hat{V} = (\eta_x/J)u + (\eta_y/J)v + (\eta_z/J)w \tag{11b}$$

$$\hat{W} = (\zeta_x/J)u + (\zeta_y/J)v + (\zeta_z/J)w \tag{11c}$$

and

$$A_{\eta\eta} = \beta_3 \rho D \left[\frac{\eta_x^2}{J} + \frac{\eta_y^2}{J} + \frac{\eta_z^2}{J} \right] \tag{12a}$$

$$A_{\zeta\zeta} = \beta_3 \rho D \left[\frac{\zeta_x^2}{J} + \frac{\zeta_y^2}{J} + \frac{\zeta_z^2}{J} \right] \tag{12b}$$

$$A_{\eta\zeta} = A_{\zeta\eta} = \beta_3 \rho D \left[\frac{\eta_x \zeta_x}{J} + \frac{\eta_y \zeta_y}{J} + \frac{\eta_z \zeta_z}{J} \right] \tag{12c}$$

with the additional assumption that D is the kinematic binary diffusion coefficient. Since the gas is assumed to be a mixture of thermally perfect gases, the equation of state follows from Dalton's law of partial pressures

$$p = \frac{\beta_1 \rho T}{\mathcal{M}} \tag{13}$$

where

$$\mathcal{M} = \left(\sum_{s=1}^{n} \frac{c_s}{\mathcal{M}_s} \right)^{-1} \tag{14a}$$

$$\beta_1 = \frac{\tilde{R}_u \tilde{T}_\infty}{\tilde{\mathcal{M}}_\infty \tilde{V}_\infty^2} \tag{14b}$$

and $\mathcal{M}$ is the mixture molecular weight, $\mathcal{M}_s$ the species molecular weight, and $\tilde{R}_u$ the universal gas constant [8314.34 J/(kmol · K)]. The alternate form of the equation of state

$$p = (\bar{\gamma} - 1)\rho e \tag{15}$$

can now be used to compute $\bar{\gamma}$, where $\bar{\gamma}$ is defined by

$$\bar{\gamma} = h/e \tag{16}$$

In addition, the following nondimensionalizations have been employed:

$$\mathcal{M} = \frac{\tilde{\mathcal{M}}}{\tilde{\mathcal{M}}_\infty} \tag{17a}$$

$$C_{pf} = \frac{\tilde{C}_{pf} \tilde{T}_\infty}{\tilde{V}_\infty^2} \tag{17b}$$

$$\dot{\omega}_s = \frac{\tilde{\dot{\omega}}_s}{\tilde{\rho}_\infty \tilde{V}_\infty} \tag{17c}$$

$$D = \frac{\tilde{D}}{\tilde{D}_\infty} \tag{17d}$$

Chemistry Model

The chemistry model employed in this study is that of clean air consisting of seven species, including electrons, and seven reactions. This model is identical to that used by Blottner et al.[27] and Prabhu et al.[12] The constituent species are molecular oxygen (O_2), atomic oxygen (O), atomic nitrogen (N), nitric oxide (NO), nitric oxide ion (NO^+), molecular nitrogen (N_2), and electrons (e^-). The following reactions are considered:

$$O_2 + M_1 \rightleftharpoons 2O + M_1 \tag{18a}$$

$$N_2 + M_2 \rightleftharpoons 2N + M_2 \tag{18b}$$

$$N_2 + N \rightleftharpoons 2N + N \tag{18c}$$

$$NO + M_3 \rightleftharpoons N + O + M_3 \tag{18d}$$

$$NO + O \rightleftharpoons O_2 + N \tag{18e}$$

$$N_2 + O \rightleftharpoons NO + N \tag{18f}$$

$$N + O \rightleftharpoons NO^+ + e^- \tag{18g}$$

where M_1, M_2, and M_3 are catalytic third bodies. The reaction rates and the thermodynamic and transport properties are obtained from Ref. 27. Additional details can be found in Ref. 22. An 11-species air chemistry model has also been incorporated into the UPS code; however, only the results from the 7-species model are presented in this study.

Numerical Method

The algorithm used to solve the fluid dynamic equations is essentially the same as that of Lawrence et al.[24] The equations are solved in a finite-volume, upwind TVD manner. In the finite-volume method, the metrics in Eqs. (2) are replaced by the cell-face area vectors. The algorithm is second-order accurate in the crossflow plane and first-order accurate in the marching direction. Fluxes are evaluated at the $n + 1$ marching plane and linearized about the n marching plane. Approximate factorization is employed so that a block-tridiagonal system is solved in each crossplane coordinate direction. The upwind algorithm is based on Roe's steady approximate Riemann solver, which has been modified for "real gas" effects by Tannehill et al.[16,17] using the approach of Grossman and Walters.[28] The effects of mass diffusion have been included in the heat flux terms and incorporated into the algorithm in the explicit (right-hand) side only. Second-order-accurate central differences were used to model the mass diffusion terms. Details of the algorithm can be found in Refs. 17 and 24.

Numerical Solution of Species Continuity Equations

The species continuity equations are solved numerically using the loosely coupled approach in a manner similar to that of Tannehill et al.[17] The assumption of zero net charge of the gas is used to eliminate the electron mass conservation equation. In addition, the species continuity equation for N_2 is eliminated by using the requirement that the mass fractions must sum to unity:

$$c_n = 1 - \sum_{s=1}^{n-1} c_s \tag{19}$$

This leaves only five species continuity equations to be solved.

The species continuity equations are modeled using a second-order-accurate, upwind-biased TVD scheme for the convective terms and second-order-accurate central differences for the diffusion terms. If the equations are put in strong conservation-law form, the species densities are obtained directly from the solution of the species continuity equations. With the loosely coupled approach, it was observed that the sum of the species densities obtained from this form of the equations did not equal the mixture density obtained from the fluid dynamic equations. This gave rise to numerical instabilities during the coupling process. As a result, the convective terms of the species continuity equations have been modeled in nonconservation-law form, which yield the species mass fractions instead of the species densities. This approach has been found to work well. Because the convective terms are in a nonconservation-law form, it is difficult to model these terms in a finite-volume fashion. The coefficients of the convective terms are evaluated at the cell centers, whereas the derivatives are evaluated across the cell from one cell face to the other. The diffusion terms, however, are in strong

conservation-law form and are easily modeled in a finite-volume format. Although the present species continuity equations are in a nonconservation-law form, mass conservation is checked at each streamwise (marching) plane and has been satisfied for all cases in this study.

The term representing the rate of production of species, $\dot{\omega}_s$, is treated as a source term, and is lagged to the n marching level. A line Gauss-Seidel procedure with successive overrelaxation (SOR) was employed to solve each equation. A scalar tridiagonal solver was used to solve each line of the Gauss-Seidel sweep for each of the species continuity equations. Anywhere from 5 (cone at angle of attack) to 34 (generic hypersonic vehicle) iterations were needed to achieve a residual of $\varepsilon = 10^{-8}$, depending on the geometry and flow conditions. The residual is defined as

$$|c_s^{i+1} - c_s^i|_{\max} \leq \varepsilon \tag{20}$$

where $i + 1$ is the current iteration level and i the previous iteration level.

Fluid/Chemistry Coupling

The coupling between the fluids and the chemistry is performed in an approximate manner. First, a fluid step is taken from marching station n to $n + 1$ assuming frozen chemistry. Then the fluid density and velocity at $n + 1$ are used in the solution of the species continuity equations to obtain species mass fractions at $n + 1$. Finally, the species mass fractions, molecular weight of the mixture, fluid density, and internal energy at $n + 1$ are used to obtain the new pressure, temperature, $\bar{\gamma}$, specific enthalpy, and frozen specific heats at the $n + 1$ marching station.

The temperature is obtained by performing a Newton-Raphson iteration of the following form:

$$\tilde{T}^{k+1} = \tilde{T}^k - \frac{g(\tilde{T}^k) - \bar{e}}{g'(\tilde{T}^k)} \tag{21}$$

and

$$g(\tilde{T}^k) = \sum_{s=1}^{n} c_s \left(\tilde{h}_s(\tilde{T}) - \frac{\tilde{R}_u \tilde{T})}{\tilde{M}_s} \right) \tag{22}$$

$$g'(\tilde{T}^k) = \sum_{s=1}^{n} c_s \left(\tilde{C}_{p,s}(\tilde{T}) - \frac{\tilde{R}_u}{\tilde{M}_s} \right) \tag{23}$$

and k is the index of the iteration. The iterations are continued until

$$|T^{k+1} - T^k| \leq \varepsilon \tag{24}$$

where ε is a small positive quantity. Once the temperature is determined, the pressure can be found from Eq. (13) and $\bar{\gamma}$ from Eq. (15). The specific enthalpy and frozen specific heats are calculated as described in Ref. 22.

The coupling between the fluids and chemistry can be enhanced through the implementation of Newton iterations on the governing equations at each streamwise step. In the Newton iteration technique, the PNS equations are written at the $n + 1$ marching station

$$\hat{E}_\xi^{n+1} + \hat{F}_\eta^{n+1} + \hat{G}_\zeta^{n+1} = 0 \tag{25}$$

and then linearized about the ith iteration level

$$(\hat{H}^{n+1})^{i+1} = (\hat{H}^{n+1})^i + \left(\frac{\partial \hat{H}^{n+1}}{\partial U} \right)^i \Delta^i U + \ldots \tag{26}$$

where

$$\hat{H} = \hat{E}, \hat{F}, \text{ or } \hat{G} \tag{27}$$

$$U = [\rho, \rho u, \rho v, \rho w, E_t]^T \tag{28}$$

$$\Delta^i U = (U^{n+1})^{i+1} - (U^{n+1})^i \tag{29}$$

The PNS equation can then be written as

$$\frac{\partial}{\partial \xi} \left[\left(\frac{\partial \hat{E}^{n+1}}{\partial U} \right)^i \Delta^i U \right] + \frac{\partial}{\partial \eta} \left[\left(\frac{\partial \hat{F}^{n+1}}{\partial U} \right)^i \Delta^i U \right] + \frac{\partial}{\partial \zeta} \left[\left(\frac{\partial \hat{G}^{n+1}}{\partial U} \right)^i \Delta^i U \right] = [-\hat{E}_\xi^{n+1} - \hat{F}_\eta^{n+1} - \hat{G}_\zeta^{n+1}]^i \tag{30}$$

In the limit of the iteration procedure, the left-hand side will go to zero (i.e., $\Delta^i U \to 0$), resulting in the solution to the nonlinear PNS equations at the $n + 1$ marching station. This procedure is similar to that used in previous studies.[8,9,29]

The iteration procedure is incorporated into the loosely coupled approach in the following manner. The PNS equations are marched from n to $n + 1$. Then the chemistry is marched from n to $n + 1$ using the fluids at $n + 1$, as previously described. Now the iterative process begins. At the $n + 1$ station, the fluids are iterated from level i to $i + 1$. The chemistry is then iterated to level $i + 1$, using the newly obtained density and velocity at station $n + 1$ and iteration level $i + 1$. All dependent variables are decoded after each iterative step. This iteration process is repeated until a desired level of convergence is achieved. At the end of each iterative step (fluids and chemistry), the species production term is re-evaluated using updated values of temperature and species densities. An added advantage of implementing the Newton iterations is that linearization and approximate factorization errors are reduced.

Numerical Results

The new three-dimensional, chemical nonequilibrium, upwind PNS code has been used to compute two test cases. The two test cases involve the three-dimensional hypersonic, laminar flow of air in chemical nonequilibrium over a sharp cone and the MDC-BWB. Wherever possible, results have been compared with other existing real gas PNS code calculations.

Test Case 1: Sharp Cone

The first test case consists of the hypersonic, laminar flow of air over a 10-deg half-angle cone at 0- and 10-deg angles of attack. The overall length of the cone is 0.5 m. The flow conditions correspond to a 8071 m/s flight velocity at an altitude of 60.96 km and are those used by Prabhu et al.[12] and Molvik and Merkle.[8] The ambient temperature and pressure at this altitude are 252.6 K and 20.35 N/m^2, respectively. These conditions result in a frozen Mach number of 25.3 and a Reynolds number of 1.29×10^5/m.

The coordinate system for this case is shown in Fig. 1. The height of the first cell at the wall was held fixed at 1.0×10^{-4} m. The outer grid height varied in the streamwise direction, with the outer grid angle set to 20 deg for the 0-deg angle-of-attack case. The wall spacing and grid height were used to determine the appropriate Roberts' stretching parameter,[30] β, for the remaining cells. As shown in Fig. 1, the ξ = const grid planes were placed normal to the x axis. The initial conditions at $x = 0.01$ m were provided by specifying freestream conditions everywhere except at the wall, where no-slip conditions and constant wall temperature were imposed. The composition (by mass) of the air was assumed to be 26.29% molecular oxygen and 73.71% molecular nitrogen. The cone wall conditions were prescribed as noncatalytic with a constant temperature of 1200 K, and the Lewis number was fixed at 1.4. The solution was marched 10 steps downstream from the initial data plane to $x = 0.011$ m with a step size of 0.0001

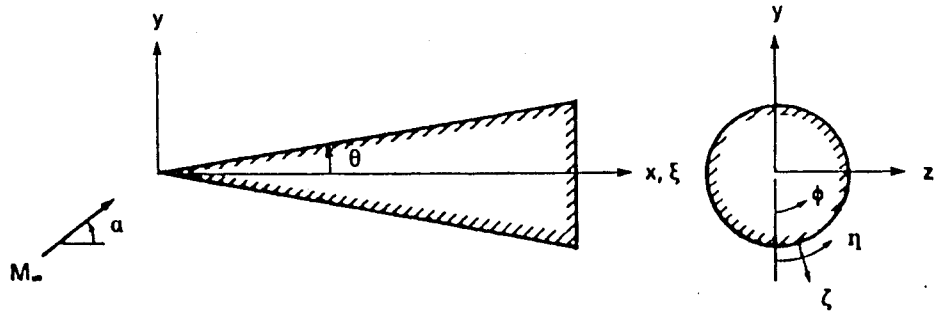

Fig. 1 Coordinate system for cone test cases.

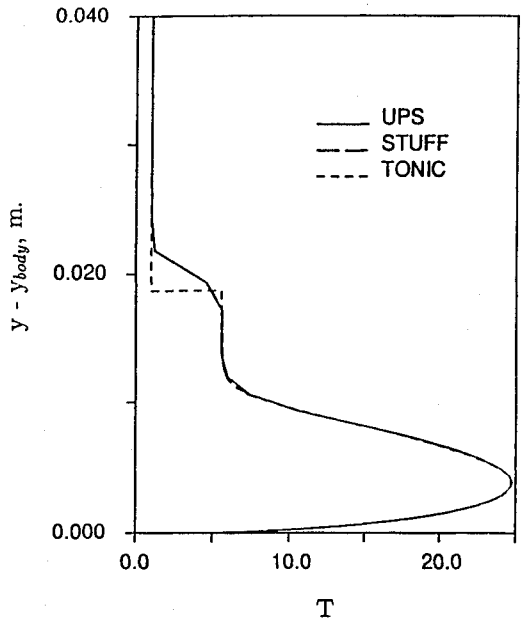

Fig. 2 Comparison of nonequilibrium sharp-cone temperature profiles at $x = 0.5$ m, $\alpha = 0$ deg.

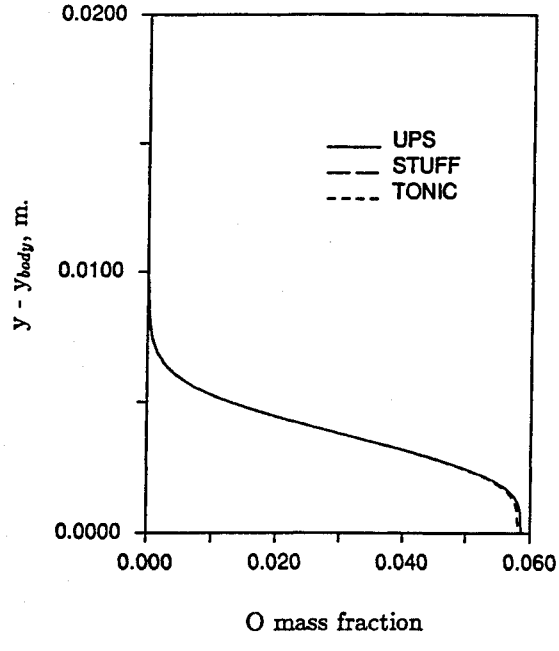

Fig. 3 Comparison of nonequilibrium sharp-cone O mass fraction profiles at $x = 0.5$ m, $\alpha = 0$ deg.

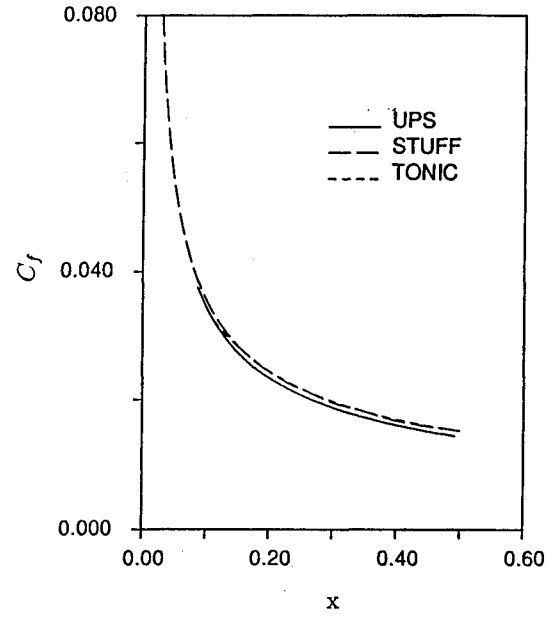

Fig. 4 Comparison of nonequilibrium sharp-cone skin-friction coefficients, $\alpha = 0$ deg.

m. This solution then served as a starting point for the final run where the solution was marched downstream to $x = 0.5$ m with a constant step size of 0.001 m.

The temperature profile for the 0-deg angle-of-attack case is compared with results from the fully coupled, upwind STUFF code of Molvik and Merkle[8] and the fully coupled, shock-fitting TONIC code of Prabhu et al.[11,12] and Wadawadigi[25] in Fig. 2 at $x = 0.5$ m. The comparison is excellent throughout the shock layer. The superior ability of the shock-fitting TONIC code in modeling the shock can be seen clearly. The atomic oxygen (O) mass fraction profile at $x = 0.5$ m is compared in Fig. 3. The comparison is good, with minor differences observed in the near-wall region. The remainder of the species agreed in a similar manner and are not presented here. Streamwise variations of skin friction and heat transfer coefficients are presented in Figs. 4 and 5. These coefficients compare well among the three codes. Slight oscillations in the streamwise variation of heat transfer are present in the STUFF results. This behavior is believed to be due to the motion of the shock across grid lines in this upwind shock-capturing code. As the shock wave moves oblique to the nearly aligned grid, it "jumps" from one grid line to the next. This has been observed (in severe cases) to spawn nonphysical waves that propagate toward the body surface in both the STUFF and UPS codes. This behavior can be suppressed by introducing some numerical dissipation at the shock; however, this tends to broaden the shock structure by approximately one more interior point. Figure 6 shows a comparison of the tempera-

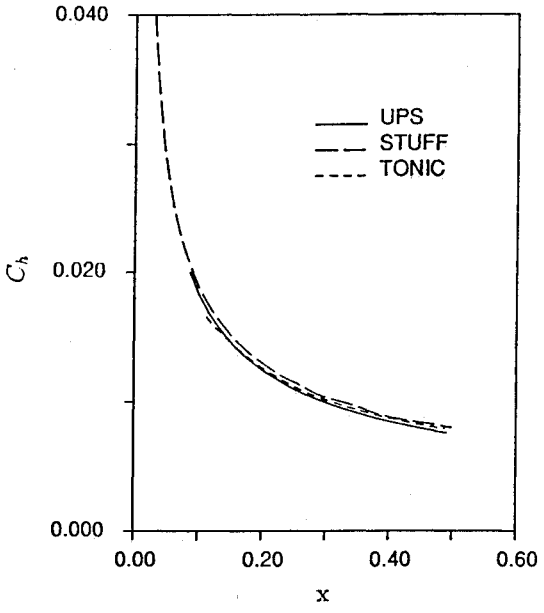

Fig. 5 Comparison of nonequilibrium sharp-cone heat transfer coefficients, $\alpha = 0$ deg.

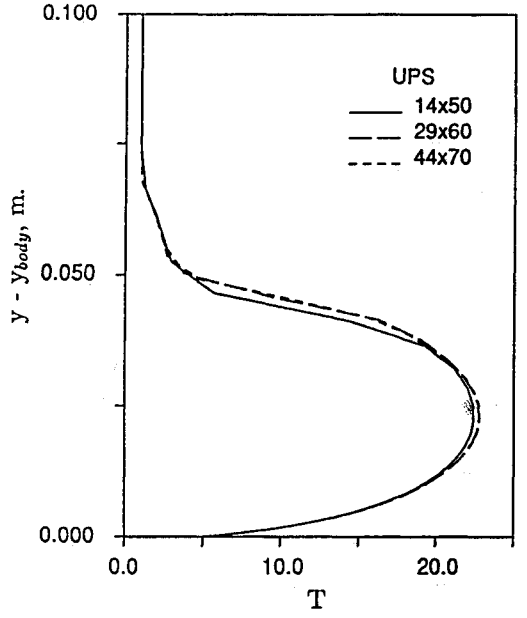

Fig. 7 Grid refinement: nonequilibrium sharp-cone leeside temperature profiles at $x = 0.5$ m, $\alpha = 10$ deg.

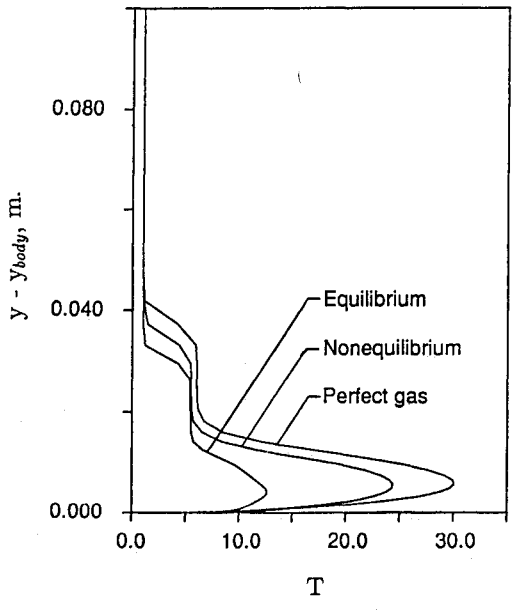

Fig. 6 Comparison of temperature profiles for perfect gas, equilibrium, and nonequilibrium chemistry at $x = 1.0$ m, $\alpha = 0$ deg.

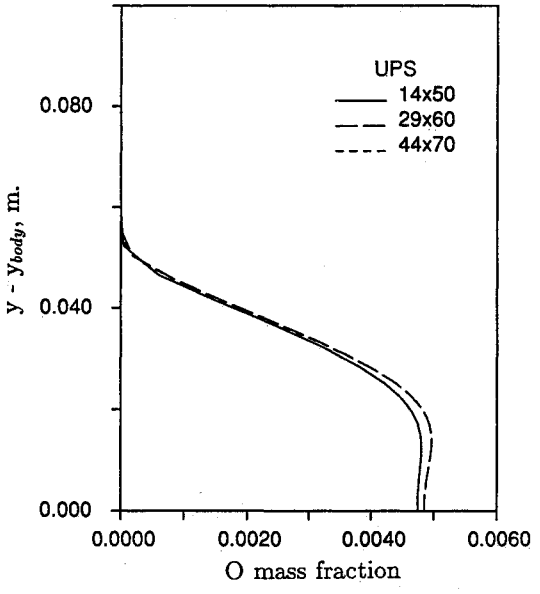

Fig. 8 Grid refinement: nonequilibrium sharp-cone leeside O mass fraction profiles at $x = 0.5$ m, $\alpha = 10$ deg.

ture profiles obtained using the three gas models (perfect gas, equilibrium air, nonequilibrium air) in the present code for the 0-deg angle-of-attack case at $x = 1.0$ m. As expected, the nonequilibrium results (finite-rate air) lie between those of perfect gas (frozen chemistry) and equilibrium air (infinite-rate chemical reactions).

For the 10-deg angle-of-attack case, the freestream parameters and the starting procedure were the same as for the 0-deg angle-of-attack case. The outer grid angle on the leeside of the cone was set to 35 deg, and on the windside it was set to 15 deg. A grid-refinement study was performed for this angle-of-attack case. Three grids were employed: coarse (14 × 50), medium (29 × 60), and fine (44 × 70), where the first number indicates the number of circumferential cells and the second number indicates the number of radial cells. The wall spacing was kept fixed at a value of 1.0×10^{-4} m. The leeside temperature profile is shown in Fig. 7, and indicates little variation between the medium- and fine-grid solutions. However, there is an observable difference between the coarse and medium grids. The leeside profile of atomic oxygen (O) is shown in Fig. 8. Again, there is an observable difference between the coarse and medium grids, and very little difference between the medium and fine grids. The fluid properties on the windside of the cone showed no variation with respect to the grid refinement, and the species profiles displayed the same behavior as the leeside profiles. As a result of this grid-refinement study, comparisons were made with STUFF and TONIC using the fine (44 × 70) grid. The TONIC code, however, was executed with only 51 points in the radial direction because it is a shock-fitting code. It was found that this number of grid points gave approximately the same number of points within the shock layer as the present code when using the fine grid.

The effect of Newton iterations was also investigated. Only minor graphical differences (less than 1%) could be observed in the fluid and species profiles with respect to the number

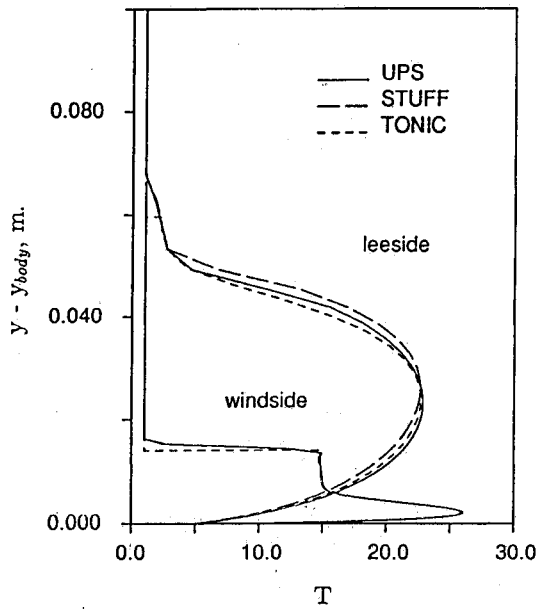

Fig. 9 Comparison of nonequilibrium sharp-cone temperature profiles at x = 0.5 m, α = 10 deg.

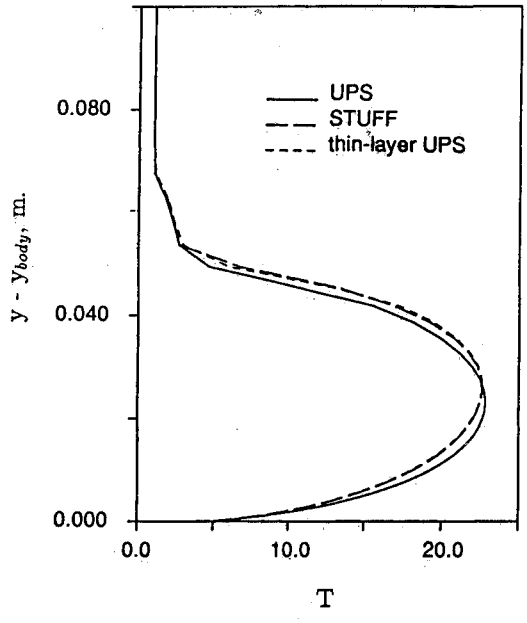

Fig. 10 Effect of thin-layer approximation on nonequilibrium sharp-cone leeside temperature profiles at x = 0.5 m, α = 10 deg.

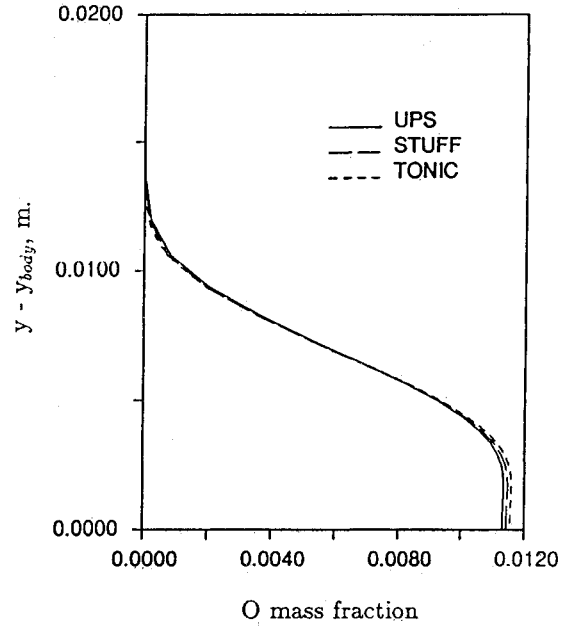

Fig. 11 Comparison of nonequilibrium sharp-cone windside O mass fraction profiles at x = 0.5 m, α = 10 deg.

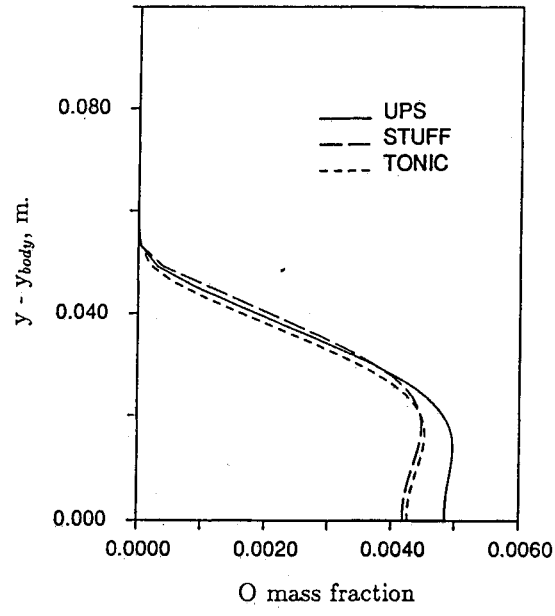

Fig. 12 Comparison of nonequilibrium sharp-cone leeside O mass fraction profiles at x = 0.5 m, α = 10 deg.

of iterations. Most of these differences are believed to be due to a reduction in the approximate factorization and linearization errors and not an improvement in the fluid/chemistry coupling, since the percent differences are of the same order as for the fully coupled STUFF code results with Newton iterations. As a result of this study, the final results were computed with no Newton iterations.

The windside and leeside profiles of temperature at x = 0.5 m are compared in Fig. 9. The windside profile is in excellent agreement throughout the shock layer. The leeside profile shows a good comparison. The differences between the present results and those of STUFF were found to be due primarily to the differences in the equations that are being solved. The STUFF code solves the thin-layer form of the PNS (gasdynamic and species) equations, whereas the present code solves the full PNS equations (no thin-layer approximation). This has been investigated by reducing the present code to a thin-layer form and comparing the resulting solutions with the STUFF code solutions. Figure 10 shows a comparison of the leeside temperature profile at x = 0.5 m for STUFF, and the full PNS and thin-layer PNS versions of the present code. This figure clearly indicates that the thin-layer approximation to the PNS equations is a dominant factor in the differences between STUFF and the present results, for the leeside fluid profiles. Differences between the present results and TONIC are believed to be due to the fact that the TCNIC code is a thin-layer PNS, centrally differenced, finite-difference code, where the metrics are not modeled in a conservative fashion. Whereas, the present code is an upwind, finite-volume code that is conservative and does not require the addition of artificial smoothing terms.

Atomic oxygen (O) mass fraction profiles for the windside and leeside of the cone are compared in Figs. 11 and 12 at x = 0.5 m. The windside comparison shows excellent agree-

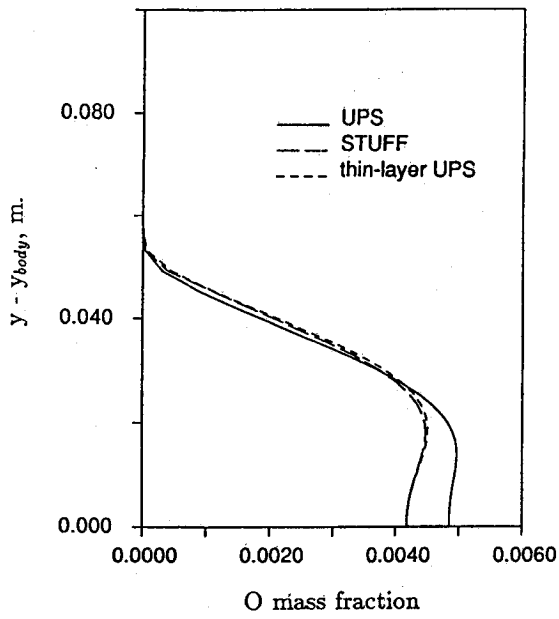

Fig. 13 Effect of thin-layer approximation on nonequilibrium sharp-cone leeside O mass fraction profiles at $x = 0.5$ m, $\alpha = 10$ deg.

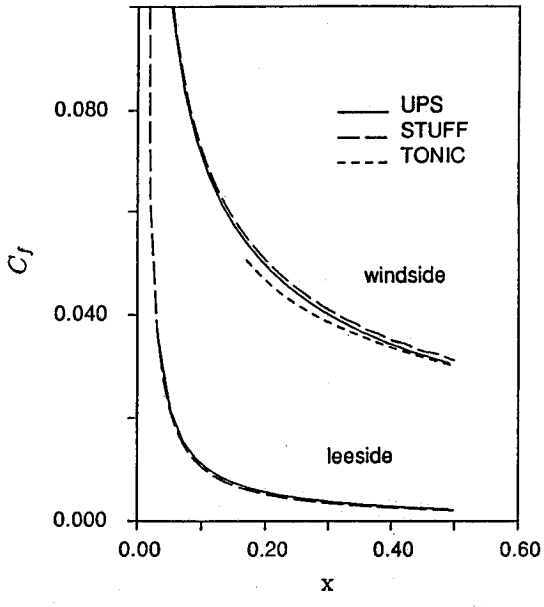

Fig. 14 Comparison of nonequilibrium sharp-cone skin-friction coefficients, $\alpha = 10$ deg.

ment among the three codes; however, the leeside exhibits noticeable differences. Again, this can be explained by the fact that TONIC and STUFF are both thin-layer PNS codes and the present code is a full PNS code. Figure 13 shows a comparison of the leeside species profile for STUFF, and the full PNS and thin-layer PNS versions of the present code. The effect of the thin-layer approximation is clearly evident.

Streamwise variations of skin friction and heat transfer coefficients for the windside and leeside of the cone are presented in Figs. 14 and 15. The leeside comparison shows excellent agreement among the three codes. The comparison of the windside skin friction and heat transfer coefficients is good and improves as one proceeds downstream. Additional results for the 0- and 10-deg angle-of-attack cone calculations can be found in Refs. 22 and 31.

Test Case 2: Generic Hypersonic Vehicle

The second test case is the Mach 25 laminar flow of air over a generic hypersonic vehicle at 0-deg angle of attack. This

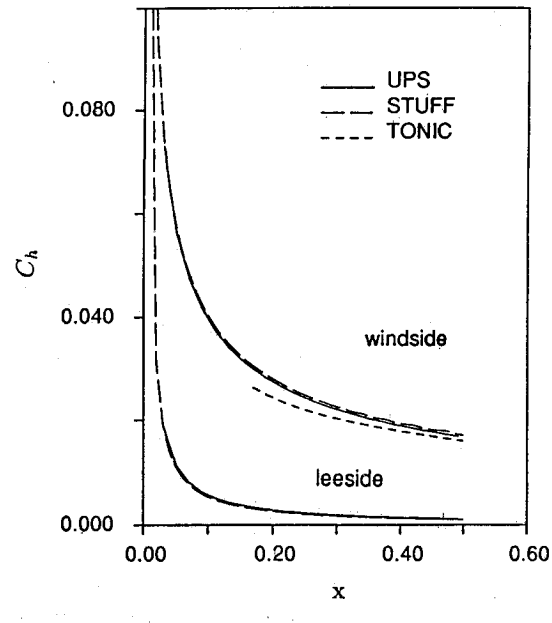

Fig. 15 Comparison of nonequilibrium sharp-cone heat transfer coefficients, $\alpha = 10$ deg.

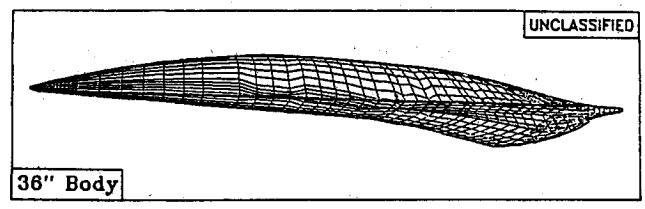

Fig. 16 Wire-frame geometry for the MDC-BWB.

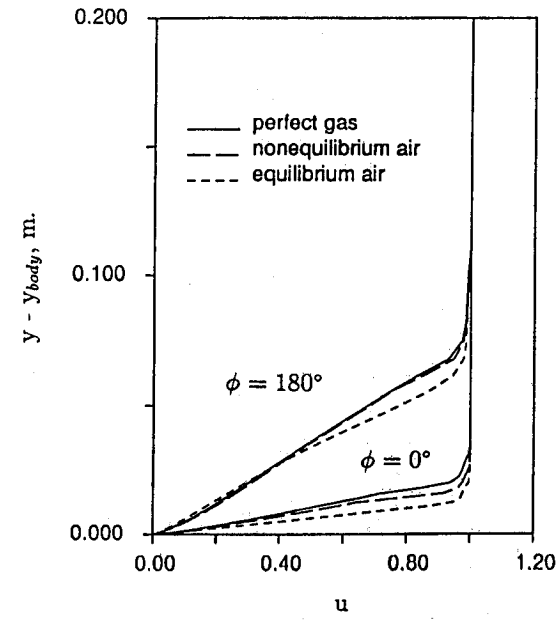

Fig. 17 Comparison of velocity profiles on the lower and upper surface symmetry planes of the MDC-BWB using the perfect gas, equilibrium, and nonequilibrium chemistry models at $x = 0.71$ m.

case was computed using the three gas models present in the code: 1) perfect gas, 2) equilibrium air, and 3) chemical nonequilibrium air. The geometry for the vehicle is the MDC-BWB (the same as that used in Ref. 32). The flow conditions are identical to those in test case 1. These conditions correspond to an altitude of approximately 61 km. A noncatalytic boundary condition was used for the species at the wall, and

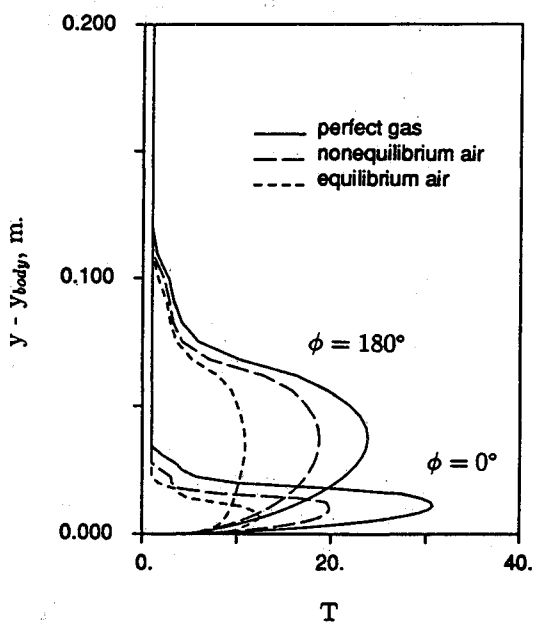

Fig. 18 Comparison of temperature profiles on the lower and upper surface symmetry planes of the MDC-BWB using the perfect gas, equilibrium, and nonequilibrium chemistry models at x = 0.71 m.

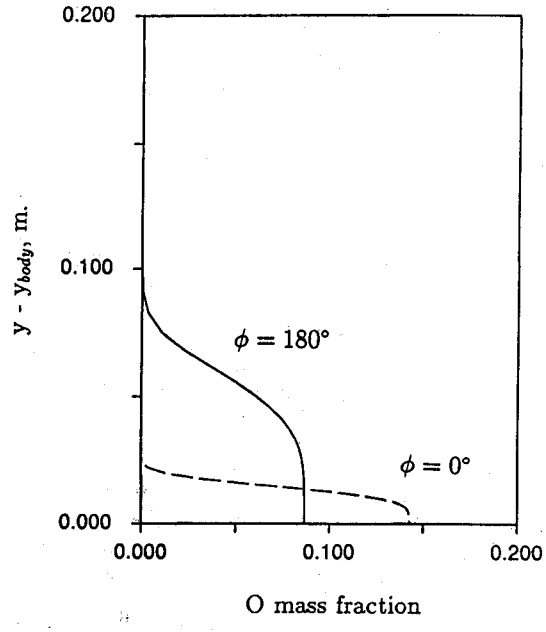

Fig. 19 O mass fraction profiles on the lower and upper surface symmetry planes of the MDC-BWB at x = 0.71 m.

the wall temperature was fixed at 1200 K. The algebraic grid consisted of 64 cells in the radial direction and 64 cells in the circumferential direction. The basic wire-frame geometry is shown in Fig. 16. The initial conditions at x = 0.038 m were obtained by using the step-back procedure within the code. The solution was then marched downstream with a step size of 2.54×10^{-4} m for the perfect gas and equilibrium cases, and 1.27×10^{-4} m for the nonequilibrium case.

The velocity and temperature profiles for the three gas models are shown in Figs. 17 and 18 at x = 0.71 m. These figures show profiles at the lower (ϕ = 0 deg) and upper (ϕ = 180 deg) surface symmetry planes. As expected, the chemical nonequilibrium (finite-rate chemical reactions) results lie between the perfect gas (frozen chemistry) and equilibrium (infinite-rate chemical reactions) results. The profiles of O mass fractions on the lower and upper surface symmetry planes at x = 0.71 m are shown in Fig. 19 for the chemical nonequilibrium case. Further results, including cross-section and symmetry plane contours, are presented in Ref. 22. All results for the MDC-BWB were obtained with an earlier version of the code that employed a first-order-accurate representation of the convective terms in the species continuity equations.

Preliminary code calculations were performed on an Apollo DN3500 engineering workstation located at Iowa State University. The perfect gas, equilibrium air, and nonequilibrium air computations required 0.028, 0.033, and 0.059 s/step/grid cell, respectively. All of the final computations were performed on the Cray YMP located at the Numerical Aerodynamic Simulation Facility at NASA Ames Research Center.

Concluding Remarks

A new chemical nonequilibrium, upwind, parabolized Navier-Stokes (PNS) code has been developed to compute the three-dimensional flow of air around hypersonic vehicles. The code is an extension of the three-dimensional UPS code of Lawrence et al. The fluid dynamic and the chemistry equations are solved in a loosely coupled manner. The code is capable of solving perfect gas, equilibrium air, or chemical nonequilibrium airflows by changing just one input parameter. The code has been used to compute the Mach 25 laminar flow of air in chemical equilibrium and nonequilibrium over a 10-deg half-angle sharp cone at 0- and 10-deg angles of attack. The results of these computations are in good agreement with those obtained from existing upwind and central-difference "real gas" PNS codes. For the nonequilibrium calculation of the sharp cone at angle of attack, it was observed that the solution of the full PNS equations was noticeably different from the solution of the thin-layer PNS equations. Also for the cases considered in this study, the loosely coupled approach was found to give sufficient fluid/chemistry coupling without the need for Newton iterations. Finally, solutions have been obtained for the McDonnell Douglas Blended-Wing-Body generic option hypersonic vehicle using the three gas model options available in the present code.

Acknowledgments

This work was supported by the NASA Ames Research Center through a Small Business Innovation Research contract (NAS2-12861). The technical monitor for this contract is Dr. Terry L. Holst. Computational resources were provided by the Numerical Aerodynamic Simulation Facility at NASA Ames Research Center and by Iowa State University. The authors wish to thank Dr. Greg A. Molvik of the Murugan Computational Aerothermodynamics (MCAT) Institute at NASA Ames Research Center for providing the STUFF code, and Ganesh Wadawadigi of Iowa State University for providing the TONIC code.

References

[1]Gnoffo, P. A., and McCandless, R. S., "Three-Dimensional AOTV Flowfields in Chemical Nonequilibrium," AIAA Paper 86-0230, Jan. 1986.

[2]Candler, G. V., and MacCormack, R. W., "The Computation of Hypersonic Ionized Flows in Chemical and Thermal Nonequilibrium," AIAA Paper 88-0511, Jan. 1988.

[3]Palaniswamy, S., Chakravarthy, S. R., and Ota, D. K., "Finite Rate Chemistry for USA-Series Codes: Formulation and Applications," AIAA Paper 89-0200, Jan. 1989.

[4]Shuen, J.-S., and Liou, M.-S., "Flux-Splitting Algorithms for Two-Dimensional Viscous Flows with Finite-Rate Chemistry," AIAA Paper 89-0388, Jan. 1989.

[5]Yu, S.-T., Tsai, Y.-L. P., and Shuen, J.-S., "Three-Dimensional Calculation of Supersonic Reacting Flows Using an LU Scheme," AIAA Paper 89-0391, Jan. 1989.

[6]Palmer, G., "An Efficient, Explicit Finite-Rate Algorithm to Compute Flows in Chemical Nonequilibrium," AIAA Paper 89-0522, Jan. 1989.

[7]Hoffman, J. J., "Development of an Algorithm for the Three-Dimensional Fully-Coupled Navier-Stokes Equations with Finite-Rate Chemistry," AIAA Paper 89-0670, Jan. 1989.

[8]Molvik, G. A., and Merkle, C. L., "A Set of Strongly-Coupled Upwind Algorithms for Computing Flows in Chemical Nonequilibrium," AIAA Paper 89-0199, Jan. 1989.

[9]Bhutta, B. A., Lewis, C. H., and Kautz, F. A., II, "A Fast Fully-Iterative Parabolized Navier-Stokes Scheme for Chemically-Reacting Reentry Flows," AIAA Paper 85-0926, June 1985.

[10]Bhutta, B. A., and Lewis, C. H., "Three-Dimensional Hypersonic Nonequilibrium Flows at Large Angles of Attack," *Journal of Spacecraft and Rockets*, Vol. 26, No. 3, 1989, pp. 158–166.

[11]Prabhu, D. K., Tannehill, J. C., and Marvin, J. G., "A New PNS Code for Chemical Nonequilibrium Flows," *AIAA Journal*, Vol. 26, No. 7, 1988, pp. 808–815.

[12]Prabhu, D. K., Tannehill, J. C., and Marvin, J. G., "A New PNS Code for Three-Dimensional Chemically Reacting Flows," *Journal of Thermophysics and Heat Transfer*, Vol. 4, No. 3, 1990, pp. 257–258.

[13]Sinha, N., Dash, S. M., and Krawczyk, W. J., "Inclusion of Chemical Kinetics into Beam-Warming Based PNS Model for Hypersonic Propulsion Applications," AIAA Paper 87-1898, June 1987.

[14]Korte, J. J., and McRae, D. S., "Explicit Upwind Algorithm for the Parabolized Navier-Stokes Equations," AIAA Paper 88-0716, Jan. 1988.

[15]Chitsomboon, T., and Northam, G. B., "A 3D-PNS Computer Code for the Calculation of Supersonic Combusting Flows," AIAA Paper 88-0438, Jan. 1988.

[16]Tannehill, J. C., Ievalts, J. O., and Lawrence, S. L., "An Upwind Parabolized Navier-Stokes Code for Real Gas Flows," AIAA Paper 88-0713, Jan. 1988.

[17]Tannehill, J. C., Ievalts, J. O., Buelow, P. E., Prabhu, D. K., and Lawrence, S. L., "Upwind Parabolized Navier-Stokes Code for Chemically Reacting Flows," *Journal of Thermophysics and Heat Transfer*, Vol. 4, No. 2, 1990, pp. 149–156.

[18]Gielda, T. P., and Agarwal, R. K., "Efficient Finite-Volume Parabolized Navier-Stokes Solutions for Three-Dimensional, Hypersonic, Chemically Reacting Flowfields," AIAA Paper 89-0103, Jan. 1989.

[19]Kamath, H., "Parabolized Navier-Stokes Algorithm for Chemically Reacting Flows," AIAA Paper 89-0386, Jan. 1989.

[20]Liou, M.-F., "Three Dimensional PNS Solutions of Hypersonic Internal Flows with Equilibrium Chemistry," AIAA Paper 89-0002, Jan. 1989.

[21]Tannehill, J. C., Buelow, P. E., Ievalts, J. O., and Lawrence, S. L., "Three-Dimensional Upwind Parabolized Navier-Stokes Code for Real Gas Flows," *Journal of Spacecraft and Rockets*, Vol. 27, No. 2, 1990, pp. 150–159.

[22]Buelow, P. E., Tannehill, J. C., Ievalts, J. O., and Lawrence, S. L., "A Three-Dimensional Upwind Parabolized Navier-Stokes Code for Chemically Reacting Flows," AIAA Paper 90-0394, Jan. 1990.

[23]Lawrence, S. L., Tannehill, J. C., and Chaussee, D. S., "Upwind Algorithm for the Parabolized Navier-Stokes Equations," *AIAA Journal*, Vol. 27, No. 9, 1989, pp. 1175–1183.

[24]Lawrence, S. L., Chaussee, D. S., and Tannehill, J. C., "Application of an Upwind Algorithm to the Three-Dimensional Parabolized Navier-Stokes Equations," *AIAA Journal*, Vol. 28, No. 6, 1990, pp. 971–972.

[25]Wadawadigi, G., "Computation of Three-Dimensional Chemically Reacting Flows Using a Fully-Coupled, Shock-Fitting PNS Code," M.S. Thesis, Iowa State Univ., Ames, IA, Dec. 1989.

[26]Vigneron, Y. C., Rakich, J. V., and Tannehill, J. C., "Calculation of Supersonic Viscous Flow Over Delta Wings with Sharp Subsonic Leading Edges," AIAA Paper 78-1137, July 1978.

[27]Blottner, F. G., Johnson, M., and Ellis, M., "Chemically Reacting Viscous Flow Program for Multi-Component Gas Mixtures," Sandia Labs., Albuquerque, NM, Rept. SC-RR-70-754, Dec. 1971.

[28]Grossman, B., and Walters, R. W., "An Analysis of Split-Flux Algorithms for Euler's Equations with Real Gases," *Proceedings of the AIAA 8th Computational Fluid Dynamics Conference*, AIAA Paper 87-1117-CP, Honolulu, Hawaii, June 1987, pp. 177–186.

[29]Rai, M. M., and Chakravarthy, S. R., "An Implicit Form for the Osher Upwind Scheme," AIAA Paper 84-0088, Jan. 1984.

[30]Anderson, D. A., Tannehill, J. C., and Pletcher, R. H., *Computational Fluid Mechanics and Heat Transfer*, Hemisphere, New York, 1984.

[31]Buelow, P. E., Ievalts, J. O., and Tannehill, J. C., "Comparison of Three-Dimensional Nonequilibrium PNS Codes," AIAA Paper 90-1572, June 1990.

[32]Richardson, P., Parlette, E., Morrison, J., Switzer, G., Dilley, A., and Eppard, W., "Heat Transfer and Pressure Comparisons Between Computation and Wind Tunnel for a Research Hypersonic Aircraft," AIAA Paper 89-0029, Jan. 1989.